A Cloud-Resolving Model with an Adaptive Vertical Grid for Boundary Layer Clouds

ROGER MARCHAND AND THOMAS ACKERMAN

Joint Institute for the Study of the Atmosphere and Ocean, University of Washington, Seattle, Washington

(Manuscript received 11 August 2010, in final form 18 November 2010)

ABSTRACT

Accurate cloud-resolving model simulations of cloud cover and cloud water content for boundary layer clouds are difficult to achieve without vertical grid spacing well below 100 m, especially for inversion-topped stratocumulus. The need for fine vertical grid spacing presents a significant impediment to global or large regional simulations using cloud-resolving models, including the Multiscale Modeling Framework (MMF), in which a two-dimensional or small three-dimensional cloud-resolving model is embedded into each grid cell of a global climate model in place of more traditional cloud parameterizations. One potential solution to this problem is to use a model with an adaptive vertical grid (i.e., a model that is able to add vertical layers where and when needed) rather than trying to use a fixed grid with fine vertical spacing throughout the boundary layer. This article examines simulations with an adaptive vertical grid for three well-studied stratocumulus cases based on observations from the second Dynamics and Chemistry of Marine Stratocumulus (DYCOMS-II) experiment, the Atlantic Stratocumulus Transition Experiment (ASTEX), and the Atlantic Trade Cumulus Experiment (ATEX). For each case, three criteria are examined for determining where to add or remove vertical layers. One criterion is based on the domain-averaged potential temperature profile; the other two are based on the ratio of the estimated subgrid-scale to total water flux and turbulent kinetic energy. The results of the adaptive vertical grid simulations are encouraging in that these simulations are able to produce results similar to simulations using fine vertical grid spacing throughout the boundary layer, while using many fewer vertical layers.

1. Introduction

Accurate cloud-resolving model (CRM) simulations of cloud cover and cloud water content for boundary layer clouds are difficult to achieve without vertical grid spacing well below 100 m, especially for inversion-topped stratocumulus. In part, this is because accurate simulation of these clouds requires accurately representing the entrainment of air into the cloud layer (Stevens et al. 2003). Bretherton et al. (1999a), for example, examined the output from 13 cloud-resolving models for a smoke cloud and found that a vertical grid spacing of 25 m produced simulations (in 1D, 2D, and 3D) with entrainment rates that were in error by more than 50% (compared with estimates extrapolated from laboratory data) while decreasing the vertical grid spacing to 5 or 12.5 m significantly reduced the scatter among models and produced lower error (between 10% and 50%).

The requirement of fine vertical grid spacing presents a significant impediment to global or large regional simulations using cloud-resolving models, including the Multiscale Modeling Framework (MMF) or superparameterization in which a two-dimensional or small three-dimensional cloud-resolving model is embedded into each grid cell of a global climate model (GCM) in place of more traditional cloud parameterizations (Randall et al. 2003; Grabowski 2001). Comparisons of MMF output from simulations with 100- to 250-m vertical grid spacing in the boundary layer (and horizontal grid spacings of 1–4 km) against observational data have shown that the MMF has a number of shortcomings, which are likely due to insufficient resolution. In particular, MMF output has been compared against retrievals from spaceborne passive imagers, such as the National Aeronautics and Space Administration (NASA) Multiangle Imaging Spectroradiometer (MISR) and against observations from the NASA CloudSat cloud radar (Zhang et al. 2008; Marchand et al. 2009; Marchand and Ackerman 2010).

Corresponding author address: Dr. Roger Marchand, Joint Institute for the Study of the Atmosphere and Ocean, University of Washington, Box 355672, 3737 Brooklyn Ave. NE, Seattle, WA 98105.
E-mail: rojmarch@u.washington.edu

DOI: 10.1175/2010JAS3638.1

These comparisons show the MMF underpredicts the occurrence of low clouds while overpredicting cloud optical depth and the occurrence of drizzle.

One potential solution to this problem is to use a model with an adaptive vertical grid (i.e., a model that is able to add vertical layers where and when needed) rather than trying to use a fixed grid with fine vertical grid spacing throughout the boundary layer. While atmospheric models more commonly use fixed grids than adaptive grids, the potential benefits of adaptive grids have attracted some attention. Much of the research in this area has focused on the application of adaptive horizontal grids for global or large regional-scale modeling (e.g., Bacon et al. 2007; Barros and Garcia 2004; Iselin et al. 2005; Jablonowski et al. 2006; Lauter et al. 2007). Examples of atmospheric models using vertical adaptive grids include Dietachmayer and Droegemeier (1992) and Fiedler and Trapp (1993), who developed the continuous dynamic grid adaption (CDGA) scheme and used this scheme to model rising thermals, and Skamarock and Klemp (1993) and Stevens and Bretherton (1999), who used an automated mesh refinement (AMR) approach in which two-way nested grids (i.e., overlying grids with differing grid spacings) are used to increase the grid spacing in a portion of the domain.

In all of these studies the authors found that model simulations with adaptive grids compared well against simulations where the same model was run with fine grid spacing throughout the domain and generally outperformed simulations run on a coarse grid from which adaptive simulation are initialized. Given the significant reductions in computational burden associated with adaptive grids (typically factors of 2–8 when compared with using fine resolution throughout the simulation domain, depending on the ratio of the starting grid to the minimum allowed grid spacing), why are adaptive grids not more widely used? There appear to be a variety of reasons, including the increased complexity of coding an adaptive scheme and concerns about the reliance of many atmospheric models on parameterizations of subgrid processes that are to some degree resolution dependent. But perhaps the most significant factor in reducing the use of adaptive grids is simply that there is no fundamental theory that describes how (or when) to reduce grid resolution, and thus all criteria are to some degree subjective. Fiedler and Trapp (1993), for example, increased grid resolution based on the value of the calculated buoyancy, while Stevens and Bretherton (1999) placed and adjusted the location of a higher-resolution subgrid based on the location of the boundary layer inversion.

To be effective in a global cloud-resolving model, the criteria for deciding when and where to reduce the grid spacing must be effective across a wide range of conditions. As a starting point, in this article we examine simulations using an adaptive vertical grid for three well-studied stratocumulus cloud cases. Model initialization and forcing data for these cases are based on observations collected during the Second Dynamics and Chemistry of Marine Stratocumulus field study (DYCOMS-II; Stevens et al. 2003), the Atlantic Stratocumulus Transition Experiment (ASTEX; Albrecht et al. 1995), and the Atlantic Trade Cumulus Experiment (ATEX; Stevens et al. 2001). These cases represent three strikingly different and climatically important stratocumulus cloud regimes. Simulations are presented using three adaptive criteria, which are described in section 2. This is followed in sections 3–5 with results for each case study. The results of the adaptive vertical grid simulations are encouraging in that these simulations are able to reproduce many features of these stratocumulus boundary layers and their temporal evolution while using only a modest number of layers as compared with simulations using fine vertical grid spacing throughout the domain. In section 6, we discuss several limitations of this study and likely directions of our future research.

2. Description of model

The cloud-resolving model used in this study is a modified version of the System for Atmospheric Modeling (SAM) cloud-resolving model (Khairoutdinov and Randall 2003). The version used here includes all updates and corrections to this model up through version 6.7 but does not include the two-moment Morrison microphysical scheme that has been added recently (starting with version 6.8.1). Rather, the model uses a simple bulk microphysics scheme in which the CRM predicts the total nonprecipitating water (vapor + liquid + ice) and total precipitating water (rain + snow + graupel), as described in detail by Khairoutdinov and Randall (2003). Cloud condensate exists whenever the total nonprecipitating water exceeds water vapor saturation. The model parameterizes subgrid-scale (SGS) transport by turbulence and subgrid total kinetic energy (TKE) using the 1.5-order turbulence closure scheme of Deardorff (1980). All of the simulations conducted here are two-dimensional using cyclic lateral boundary conditions and contain no ice condensate.

We have modified the SAM cloud resolving model to include an adaptive vertical grid (AVG). In the SAM-AVG model layers can be added or removed based on a variety criteria, which we will describe below. As a result, vertical regions with relatively fine grid spacing can shift with changes in the boundary layer structure, such as changes in the position of inversions or cloud boundaries. Layers are inserted or removed so that mass and energy are conserved. Equations are provided in the appendix.

In this article we evaluate three different criteria for determining when to insert or remove vertical layers: the first criteria is based on the potential temperature, the second on the ratio of the subgrid-scale vertical water flux to the total water flux, and the third on the ratio of the SGS to total vertical water flux and SGS to total kinetic energy.

With the potential temperature criterion, layers are inserted any time the change in the domain-averaged profile of potential temperature across a layer exceeds a fixed threshold. A layer was subsequently removed if the difference in potential temperature was less than 1/4 times this threshold. The idea behind this criterion is simply to concentrate additional layers near the cloud-top inversion. We found that our simulations were not very sensitive to the threshold so long as it was set sufficiently small to capture easily the change in potential temperature at the cloud inversion. A value of 0.5 K was used in all the simulations present here. The threshold for removing layers must be chosen to be more than a factor of ½ smaller than the threshold for adding layers; otherwise, layers will tend to be removed immediately after they are added (since the change in potential temperature across the new layer can be expected to be at least half that of the originating layer). We did not experiment with the removal criteria threshold extensively, but we found that values less than 1/3 (the threshold for adding layers) worked poorly (removing layers that are helpful) and values larger than 1/5 appeared excessively conservative (keeping layers than were not very beneficial).

With the SGS to total water flux criterion, vertical layers are added when the ratio of the total (vertical) water flux contributed by the subgrid-scale scheme to the total water flux (SGS + resolved) was larger than a fixed ratio. The motivating idea behind this criterion is simply that we want to minimize the dependence of the simulation on the subgrid-scale parameterization in favor of resolving turbulent motions. Previous research has shown that simulation of stratocumulus can a have strong sensitivity to the formulation of the subgrid parameterization (e.g., Stevens et al. 2003; Cheng et al. 2010). This point is discussed further in section 6. We found our simulation results with the SGS to total water flux criterion are somewhat sensitive to the threshold value, with values less than 10% frequently failing to add sufficient layers and values below 5% adding layers that appeared to have little benefit. All of the results presented here use a threshold value of 10%. We likewise removed layers when the ratio dropped below 1%. Again we found the results to be somewhat sensitive to this value. In general, we found keeping the removal threshold a factor of 5–10 below the insertion threshold appeared to work well. One difficulty with this approach is that in regions where the total water flux is small, the ratio of the SGS to total water flux can be larger than 10% without negatively impacting the simulation. Thus in practice we required a small minimum value for the amount of condensed water before we would insert a layer.

A third criterion that we found useful was to examine the ratio of the SGS to total kinetic energy. Overall, we found that this criterion did not work well in isolation because it does not generally cause layers to be inserted near cloud top. However, as the results in the next section will show, using this criterion in combination with the SGS to total water flux criterion proved to be useful in identifying layers in the subcloud region where additional levels are beneficial. When used in combination, we add a layer any time either criterion indicates a layer should be added and remove a layer only when both indicate it is unnecessary. As with the water flux criterion, we found the SGS to total kinetic energy criterion to be somewhat sensitive to the thresholds used. By trial, we found an insertion threshold near 20% and a removal threshold near 5% worked well for the three cases examined here.

In all three of the above approaches, we applied a variety of additional constraints to help ensure numerical stability. In particular, we did not allow the difference in the width of neighboring vertical levels to ever be more than a factor of 2. If adding a layer would violate this condition, then the neighboring layer was also reduced in size. As described in the appendix, the layer insertion technique that we used centers a new layer on the interface between two existing layers. This process reduces the size of the existing–neighboring layers, such that adding a layer does not cause this neighbor-width condition to be violated in most cases. If removing a layer would cause this condition to be violated, the layer is not removed.

In all the adaptive grid simulations shown here, we begin the simulation using a base grid with 100-m vertical spacing. Points in the base grid cannot be removed. Also, except when stated otherwise, we set the minimum thickness for any new layer to 12.5 m, corresponding to a maximum eightfold decrease in vertical grid spacing. Finally, in all the adaptive grid simulations shown we chose to add or remove layers every 5 min. In general we found that updating every 10 min worked roughly equally well, but updating on short time scales (e.g., 20 s) did not work well because of artificial mixing induced by adding and then removing a given layer (see appendix).

3. DYCOMS-II

DYCOMS-II took place during July 2001 about 500 km west-southwest of San Diego, California. The experiment included nine research aircraft flights, primarily at night (Stevens et al. 2003). The simulations examined here use

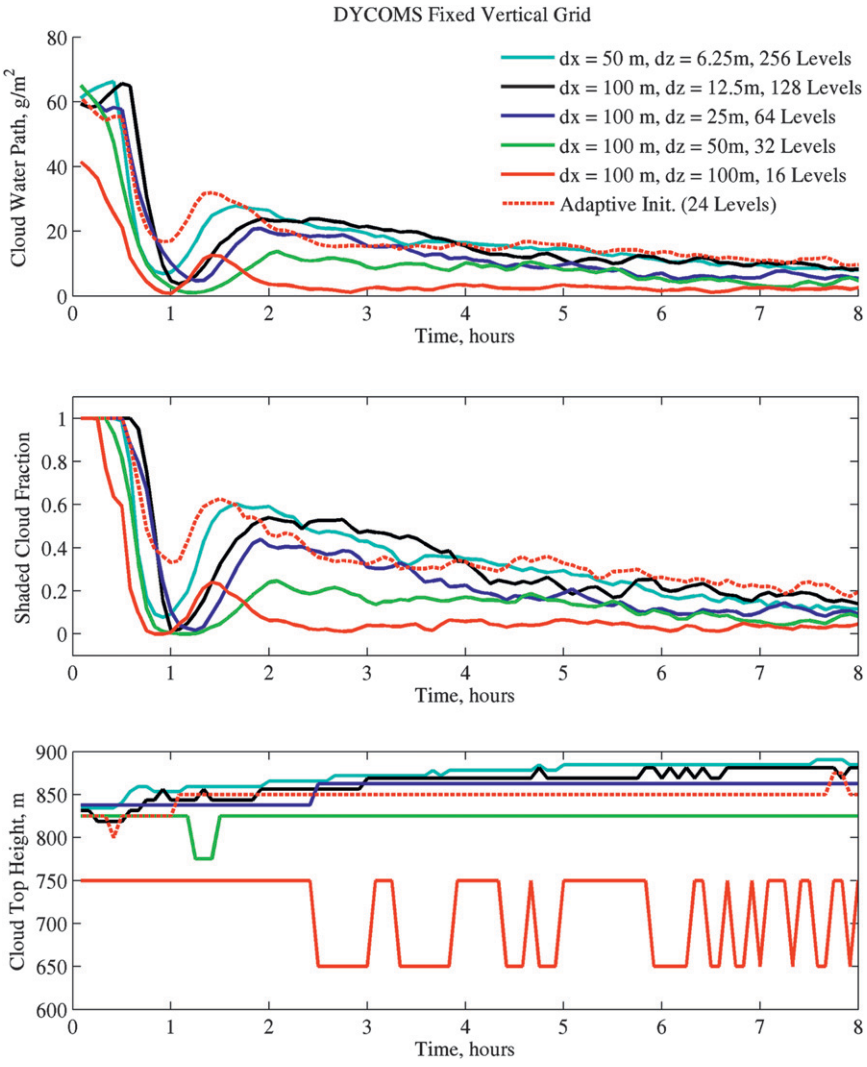

FIG. 1. Simulations of DYCOMS-II (top) cloud water path, (middle) cloud fraction, and (bottom) cloud-top height using fixed (in time) vertical grids. The horizontal and vertical grid spacing used in each simulation are listed in the figure legend. The dashed lines show results for a simulation where the vertical grid resolution is increased at the start of the simulation from 100 to 25 m where liquid water is present (see text).

initial conditions and forcings as prescribed by Stevens et al. (2005), which are based on observations from the first research flight (RF01). Stevens et al. examined output from 10 high-resolution three-dimensional models (i.e., large-eddy simulations) run using 35-m horizontal grid spacing and 5-m (or finer) vertical grid spacing. This analysis included an earlier version of the SAM model. We choose to begin our analysis with this case primarily because it focuses on a challenging nondrizzling stratocumulus near the balance point where a transition from solid to broken cloud occurs and model simulations are expected to be sensitive to vertical grid resolution.

Figure 1 shows the result of several two-dimensional SAM simulations run with fixed vertical grid spacings ranging from 100 to 6.25 m. The horizontal grid spacing for these runs was set to 100 m, except in the case where the vertical grid spacing was 6.25 m when it was reduced to 50 m. This maintains a horizontal-to-vertical grid spacing ratio of 8-to-1 or better. Our experience with this model indicates that the model produces consistent results with horizontal-to-vertical ratios less than about 10-to-1, but that larger ratios appear to artificially reduce mixing. Stevens and Bretherton (1999) also noted the tendency of very thin grid cells to reducing mixing. The domain size is set to 64 km and runs on larger domains do not produce significantly different results.

With the exception of the simulation using a 100-m vertical grid spacing, all of the model simulations initialize

with a liquid water path (vertically integrated cloud water content) of roughly 60 g m^{-2}. There is a large change in the simulated liquid water path and cloud cover in the first 2 h of the simulations, characteristic of model ''spinup.'' During the spinup, vertically averaged TKE increases as turbulent eddies develop in response to destabilization of the boundary layer. By the end of the second hour, the runs with the highest vertical resolution have liquid water paths near 25 g m^{-2} and cloud fractions near 50%. After this time, the liquid water path and cloud cover slowly decrease.

For the observational case on which the model setup was formulated (RF01), the stratocumulus cloud fraction was observed to be greater than 99% as measured by downward-pointing lidar. Aircraft in situ data indicate the cloud appeared to deepen over time, suggesting an increase in cloud water path. Many (though not all) of the models examined by Stevens et al. (2005) showed similar reductions in cloud water and cloud cover to those shown in Fig. 1. It is unclear the degree to which the cloud dissipation is a result of the spinup process rather than of the inherent dynamics of the model. In any case, our focus here is to evaluate the ability of an adaptive grid scheme to produce results consistent with those obtained from the model run at fine vertical resolution everywhere rather than to attempt to diagnose model errors. We will discuss this point further in the concluding section.

Overall, Fig. 1 shows that there is relatively little change in the simulated cloud water path or cloud cover between the simulations run with 12.5 or 6.25 m, while the cloud dissipates significantly more rapidly in those models runs with coarser vertical grid spacing. The model simulation with 100-m vertical grid spacing is particularly striking in that it initializes with notably less total cloud water than simulations with a finer vertical grid and almost entirely dissipates in the spinup phase. The difference in initial water path occurs because SAM initializes gridcell values based on the initial thermodynamic sounding at the gridcell midpoint. As it turns out, the center of the 100-m grid cell that contains cloud top (gridcell midpoint at 850 m) falls just above the position of the initial inversion (840 m) and so this layer is initialized with no cloud water. In effect, the 100-m grid discretizes the position of cloud such that it must entirely fill (or not fill) the layer between 800 and 900 m. The effect of the grid discretization is likewise evident in the bottom panel of Fig. 1, which plots the simulated cloud-top height, taken as the midpoint of the highest vertical layer that contains cloud water.

To test the sensitivity of this result to the initial water path, we modified the initial sounding profile by increasing the height of the inversion by 20 m, such that the layer between 800 and 900 m was initialized with a large cloud water content. The results of this simulation (not shown) are very similar to what is shown for the original sounding—that is, in spite of starting with too much condensed water, the cloud almost entirely dissipates during the first 2 h of the simulation.

As a second experiment, we modified the code to increase the vertical grid spacing to 25 m in any 100-m layer that contained (or was adjacent to a layer with) condensed water. This modification added eight vertical layers (to the original 16-level grid) for a total of 24 layers. The results of this simulation are given by the dotted line in Fig. 1, which is labeled ''adaptive initialization.'' The cloud water path and cloud fraction for this simulation compare favorably with those produced by the simulations using either a fixed 12.5- or 6.25-m vertical grid. The ability of the model to reproduce these particular quantities while using only a small number of additional layers was one of the factors that inspired us to examine the potential of an adaptive grid approach. While adding vertical layers only at the start of the simulation is arguably sufficient for the DYCOMS-II case, as we will see in the following section this approach is not sufficient for other cases examined because of changes in the position of the cloud with time.

Perhaps somewhat surprisingly, Fig. 1 also shows that the cloud water path and cloud fraction for the adaptive simulation (using 25-m layers only in the cloud layer) compares more favorably with the higher-resolution simulations than the simulation using 25-m vertical grid spacing throughout the boundary layer. The difference appears to be the result of decoupling of the boundary layer from the surface layer in the uniform 25-m fixed grid simulation. Figure 2 compares horizontally and temporally averaged profiles of a variety of thermodynamic variables. The figure shows that all of the simulations with evenly spaced layers and 50-m or finer vertical grid spacing feature a decoupled boundary layer as evidenced by the double-peaked structure (with a minimum below cloud base) in the profiles of vertical velocity variance and TKE. The simulation with 24 layers, however, maintains a much more well-mixed structure. Thus, while the 24-layer simulation might be expected to have a similar level of dry air entrainment from above the inversion, the cloud water in the 24-layer simulation is more readily replenished from the surface. Arguably this occurs because with 100-m grid spacing in the subcloud layer, the CRM cannot produce a resolved-scale near-surface convective layer and instead the flux is carried up with significant help from the SGS scheme.

Figure 2 also shows that the simulations with finer vertical grid spacing rely less heavily on the subgrid-scale turbulence parameterization as indicated in the rightmost panels, which show the ratio of (top) the subgrid-scale to

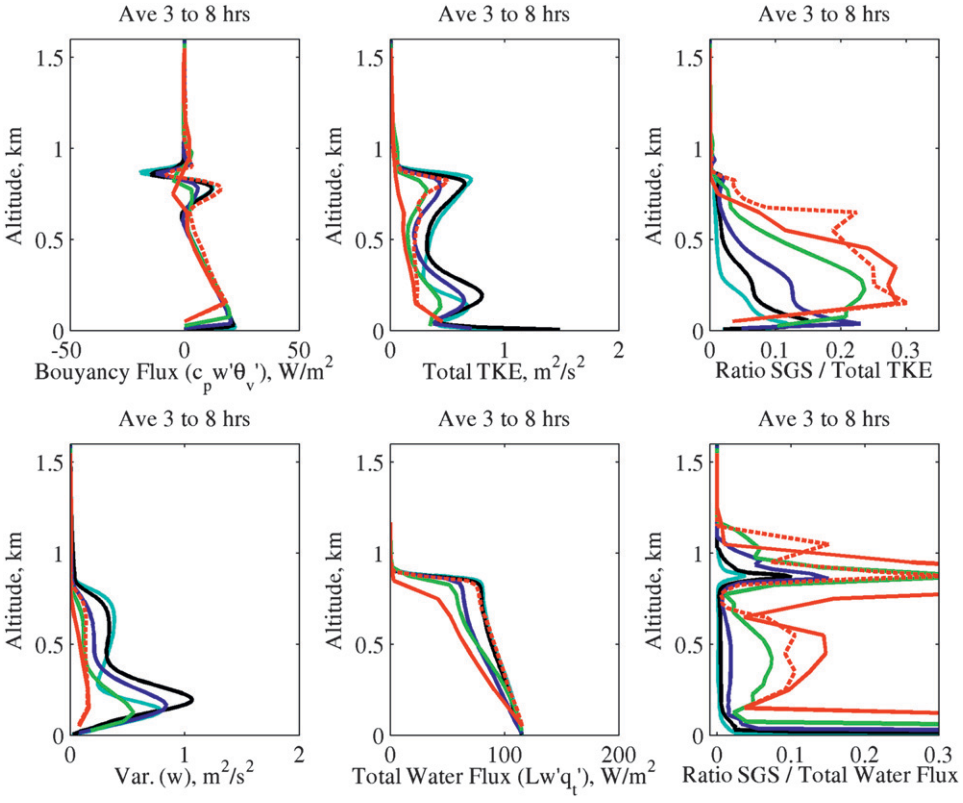

FIG. 2. Simulated profiles of (left to right) (top) buoyancy flux, TKE, ratio of subgrid-scale to total kinetic energy; (bottom) variance in vertical velocity, total water flux, and ratio of subgrid-scale to total water flux for simulation using fixed vertical grids. Profiles are averages taken over the last 5 h of the simulation. Lines are as in Fig. 1.

total TKE and (bottom) total water vertical flux. In the simulations with 12.5- and 6.25-m vertical grid spacing, the subgrid scheme represents less than 20% of TKE (with a maximum near the surface) and 10% for total water flux (except in the surface layer).

Figure 3 shows simulation results for this same case using the adaptive grid version of the model (SAM-AVG) with the three different adaptive criteria described in section 2. In each of the adaptive simulations, the initial vertical grid has 24 layers (with 25-m vertical grid spacing within the initial cloud layer and 100-m spacing outside of the cloud, following the adaptive initialization described above). The horizontal grid spacing is 100 m and the domain size is 64 km. The adaptive grid simulations permit a maximum eightfold improvement in the vertical grid spacing (to 12.5 m). The temporal change in the total number of layers and the position of layers is summarized in Fig. 4. The simulation using the potential temperature criterion (green dashed line) generates the smallest number of additional layers and these layers are concentrated near cloud top. The SGS-to-total vertical water flux criterion (blue dashed line) produces slightly more layers, placing layers throughout region occupied by the cloud layer with a concentration near cloud top and cloud base. The simulation using the SGS-to-total TKE and water flux criteria (red dashed line) uses yet more layers. Many of these layers are placed in the subcloud region, including a large number of layers near the surface.

As Fig. 3 indicates, all three of the adaptive grid solutions generate domain averaged cloud water paths, cloud fractions, and cloud-top heights that are similar to the simulation with fixed 12.5-m vertical grid spacing. The change in cloud-top height, in particular, is remarkably consistent. The simulation using the potential temperature criterion (green dashed line) does produce somewhat more cloud water and cloud cover than the other simulations. However, the rate of loss of cloud water and cloud cover after the model spinup is quite similar with the offset primarily generated during the model spinup. This makes it difficult to draw any firm conclusions regarding this offset. Nonetheless, the simulation using a potential temperature criterion maintains a relatively well-mixed boundary layer (see Fig. 5) and we speculate that this is a significant factor in this simulation retaining more cloud water. Figure 5 shows a similar set of domain-averaged thermodynamic profiles

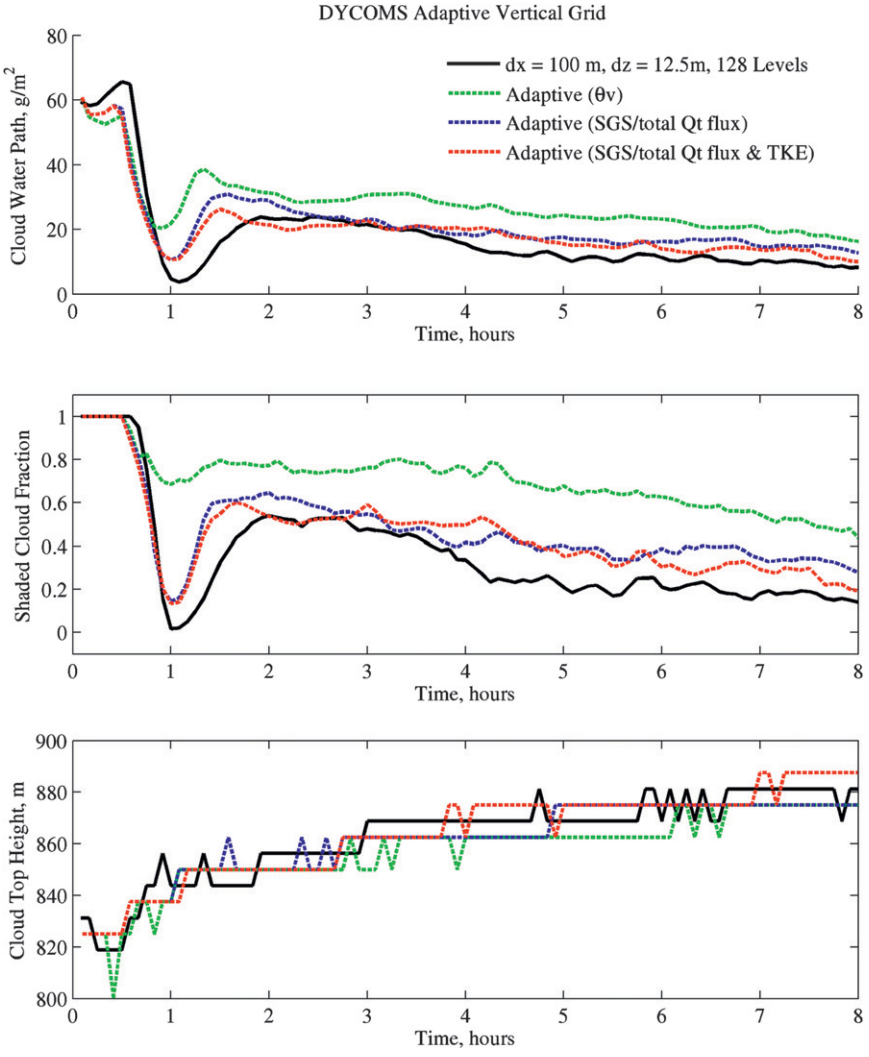

FIG. 3. Comparison of DYCOMS-II simulations of (top) cloud water path, (middle) cloud fraction, and (bottom) cloud-top height using a fixed vertical grid with a 12.5-m resolution with three adaptive vertical grid simulations. See text for description of adaptive grid criteria.

for the adaptive grid simulations, as was shown in Fig. 2 for the simulations with a fixed vertical grid. For reference, the solid black lines in Fig. 5 are for the simulation with a fixed 12.5-m vertical grid spacing. Figure 5 shows that the simulation using SGS-to-total TKE and water flux criteria is able to reproduce the structure in the subcloud layer better than the other adaptive simulations, as evidenced here by the profile of vertical velocity variance, TKE, and to a lesser degree buoyancy.

4. ASTEX

The Atlantic Stratocumulus Transition Experiment took place in the subtropical Atlantic Ocean near the Azores in June 1992 (Albrecht et al. 1995). The goal of this experiment was to study the transition from stratocumulus to subtropical trade cumulus. During ASTEX two Lagrangian experiments were carried out in which a boundary layer air mass was repeatedly sampled by aircraft as it drifted with the mean boundary layer wind. In the first ASTEX Lagrangian experiment on 12–14 June 1992, five research flights were conducted (de Roode and Duynkerke 1997). Data collected during these fights have subsequently been used in a number of modeling studies both to formulate model initializations and forcings and to evaluate model output. This includes cases based on the second research flight A209 (e.g., Khairoutdinov and Kogan 1999, 2000) and the third research flight RF06 (e.g., Duynkerke et al. 1999), as well as the full duration (Bretherton et al. 1999b).

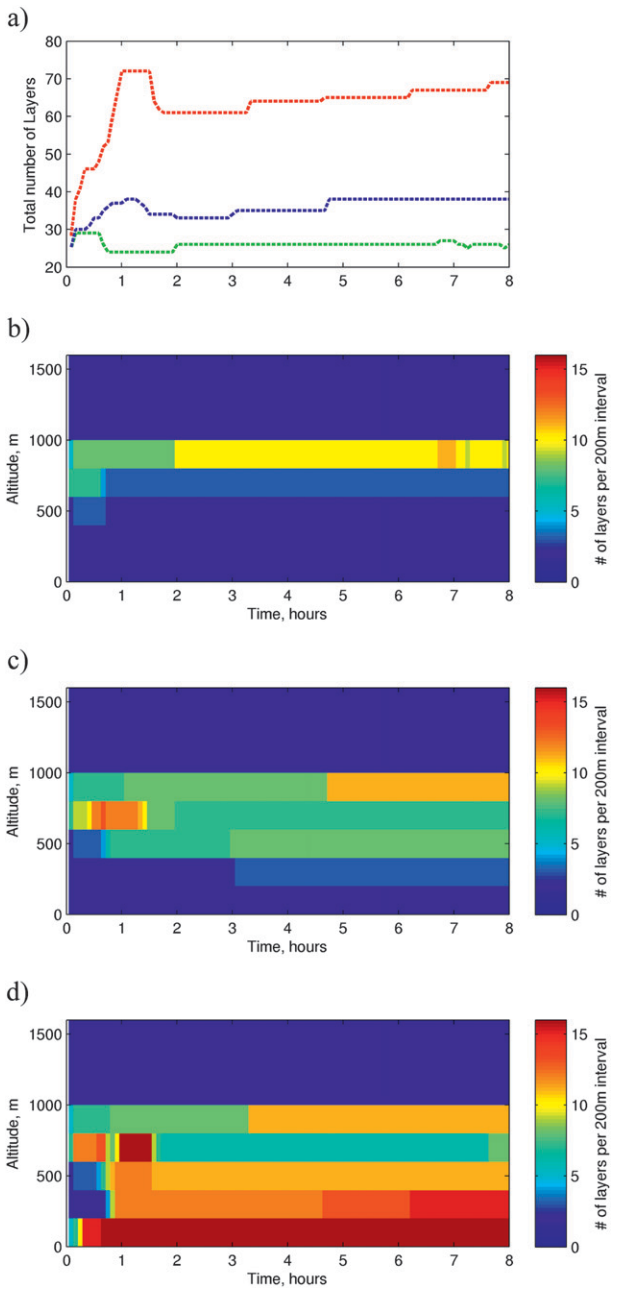

FIG. 4. Number of layers and layer concentrations for DYCOMS-II adaptive grid simulations. (a) Total number of layers used. (b)–(d) Number of layers in each 200-m interval for simulation using (b) potential temperature criterion, (c) SGS to total water flux criterion, and (d) SGS to total TKE and water flux criteria.

Here we simulate the nocturnal stratocumulus boundary layer from the second research flight (A209). We use initial thermodynamic fields and forcings as described by Khairoutdinov and Kogan (1999, 2000), which were developed based on the analysis of Duynkerke et al. (1995) and originally set up for the third Global Energy and Water Cycle Experiment (GEWEX) Cloud System Study (GCSS) boundary layer cloud workshop. Our setup differs from that of Khairoutdinov and Kogan only in that we use the simple interactive radiation scheme prescribed by Duynkerke et al. (1999) and we do not allow drizzle to form. For this case, the jump in potential temperature across the inversion is about 4 K and the observed mean liquid water content at the cloud top was about 0.6 g kg^{-1}.

As in the previous section, we begin by looking at the sensitivity of SAM simulations to vertical grid spacing. Figure 6 plots the cloud water path, cloud coverage, and cloud-top height for several simulations with fixed vertical grid spacing. The ASTEX stratocumulus cloud differs significantly from the DYCOMS-II case. The ASTEX case features stronger subsidence and a lower inversion height and contains significantly more total water. The cloud fraction for all simulations remains at or near 100% and the boundary layer remains well mixed for the first 3 h of the simulation. Except for the simulation with 100-m vertical grid spacing, there is only a small reduction in the amount of cloud liquid water during the model spinup.

Overall, Fig. 6 shows that the ASTEX simulations appear to be somewhat less sensitive to vertical grid spacing than DYCOMS-II; the ASTEX simulation with 25-m vertical grid spacing differs little from those with finer than 25-m spacing, while the DYCOMS-II case required 12.5 m to achieve convergence in this way. The ASTEX case also differs from DYCOMS-II in that the adaptive-initialization simulation (where the initial vertical grid spacing is increased from 100 to 25 m in the region where cloud liquid water is present at the start of the simulation) is not entirely effective. The result of the adaptive-initialization simulation is given by the red dotted line in Fig. 6. While the adaptive-initialization simulation compares favorably to the fixed 25-m grid simulation for the first 1.5 h, the solution diverges radically after this time. This occurs because the cloud-top height (Fig. 6c) increases significantly for this case and after 1.5 h the cloud expands into the space where the vertical grid resolution is poor (100 m).

In contrast to the adaptive-initialization approach, simulations using the full adaptive criteria are able to adjust to the change in cloud-top height as shown in Fig. 7 (bottom panel), which compares the simulated cloud-top height for the three adaptive criteria with the 12.5-m fixed vertical grid result. Likewise, an examination of the vertical layer location in the adaptive simulations (Fig. 8) shows how all three simulations shift the region where vertical layers are concentrated over time.

Overall, Fig. 7 shows that all three adaptive grid simulations produce results that are quite similar to the 12.5-m fixed vertical grid simulation for the first 3–4 h of the

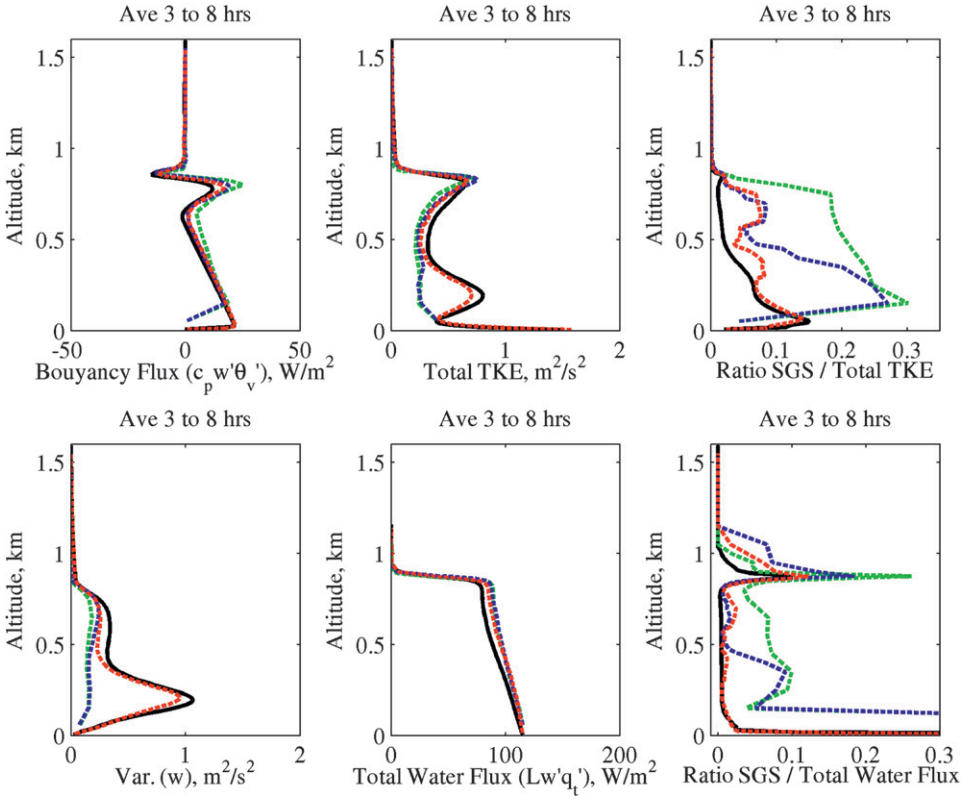

FIG. 5. Comparison of simulated profiles using a fixed vertical grid with 12.5-m spacing and three adaptive vertical grids. Profiles are averages taken over the last 5 h of the simulation. Panels are as in Fig. 2 with line colors as in Fig. 3.

simulation. After this time, the simulations using the SGS-to-total vertical water flux criterion (blue dashed line) and the potential temperature criterion (green dashed line) produce somewhat more cloud water and cloud cover. As was the case for DYCOMS-II, an examination of the model thermodynamic fields shows the boundary layer shifting from a well-mixed to a decoupled state after 3 h. Only the criterion using the SGS-to-total TKE and water flux (red dashed line) captures this change well. We will discuss the implications of this result further in section 6.

5. ATEX

The Atlantic Trade Wind Experiment took place in the subtropical Atlantic near 12°N, 35°W in February 1969. The simulations presented here use initial conditions and forcings as given by Stevens et al. (2001), which are based on observations collected during ATEX and served as a basis for analyzing model simulations run by seven different research groups. This case is of particular interest because it attempts to capture the transition from a trade cumulus regime into a stratocumulus regime. Our setup differs from that of Stevens et al. only in that our simulations are two-dimensional rather than three-dimensional and we increased the size of the domain to 320 km. This increase in domain size from the 64 km used in the DYCOMS-II and ASTEX cases was found to be necessary to ensure that there are only small variations in domain mean properties (such as the domain mean cloud water path shown in Fig. 9) and reflects the much less homogeneous nature of the ATEX cloud.

Figure 9 shows the resulting cloud water path, cloud fraction, and cloud-top height from simulations using SAM with fixed vertical grid spacings ranging from 100 to 6.25 m. Unlike the DYCOMS-II and ASTEX cases, the ATEX results are striking in that there is no convergence in the model-simulated cloud water path or cloud fraction as the vertical grid spacing is decreased. Rather, there is a strong increase in both cloud water path and cloud fraction as the grid becomes finer, as well as an increase in cloud-top height that is most evident late in the simulation. This strong sensitivity to grid spacing was identified by Stevens et al. (2001) and was explored further in a later study by Stevens et al. (2002), who examined the sensitivity of this case to both grid spacing and domain

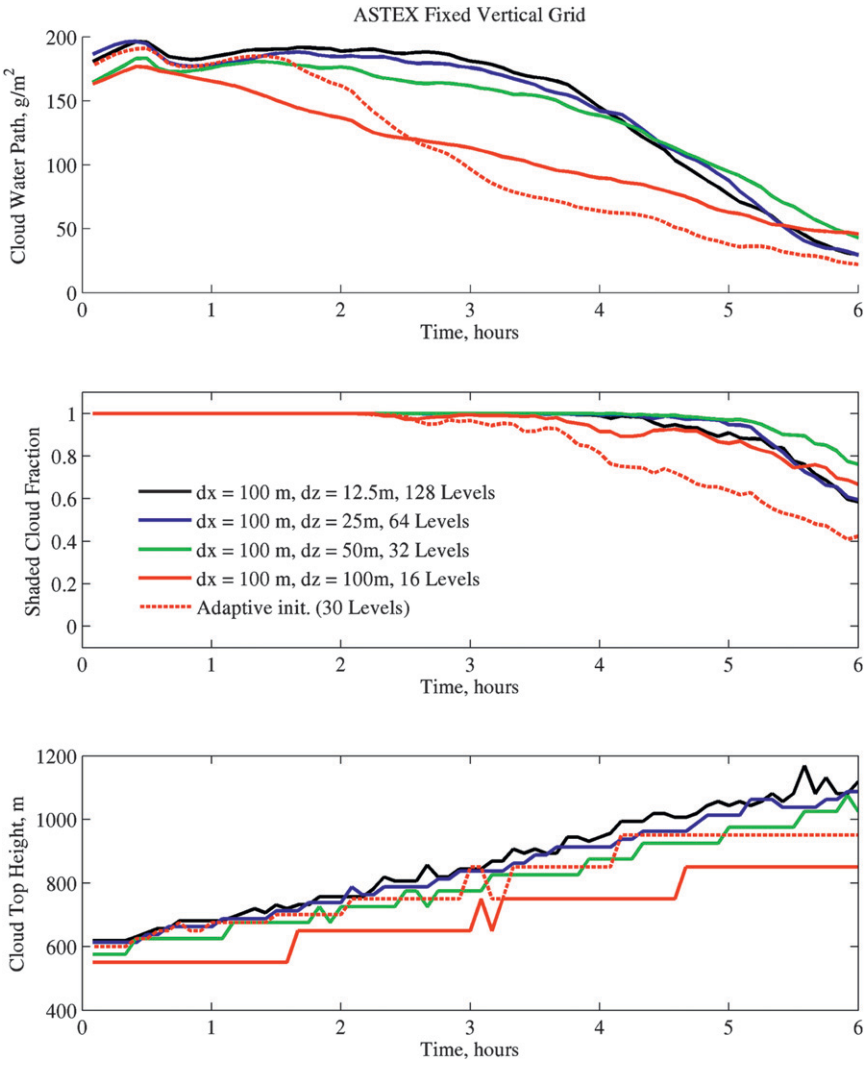

FIG. 6. As in Fig. 1, but for the ASTEX (A209) simulations.

size. The high sensitivity of this case to grid spacing appears to stem from a strong longwave cloud feedback, where simulations with finer vertical grid spacing enable the formation of more cloud cover in a thin layer near the trade inversion. This thin stratocumulus cloud leads to a large increase in longwave cooling at cloud top (which cools the atmosphere more than dry air entrainment warms it), driving stronger downdrafts and an increase in cumulus moisture flux into the stratocumulus layer, generating yet more stratocumulus.

Also unlike the DYCOMS-II and ASTEX simulations, the ATEX simulations do not initially have any cloud and it takes about 1 h before the simulation begins to develop cumulus. We found that this spinup time was somewhat sensitive (on the order of 10 min) to the details of how the small random temperature perturbations used to initialize the model are applied (e.g., size of the temperature fluctuations and the altitudes over which they are added) as well as the horizontal and vertical grid spacing. There is also some variation in spinup time from realization to realization (i.e., in response to different random perturbations in the model initialization).

Results for the adaptive grid simulations are shown in Fig. 10. In Fig. 10, the adaptive grid simulations (dashed color lines) are compared with the fixed vertical grid simulation with 12.5-m grid spacing (solid black line). All three adaptive grid simulations produce similar cloud water paths, cloud fractions, and cloud-top heights compared to the 12.5-m fixed grid simulation. During the first half of the simulation, however, the adaptive simulations produce slightly less cloud water and slightly lower cloud fractions than the fixed grid simulation. We conducted adaptive-grid simulations with 50-m horizontal grid spacing that allowed the vertical grid to be reduced to 6.25 m.

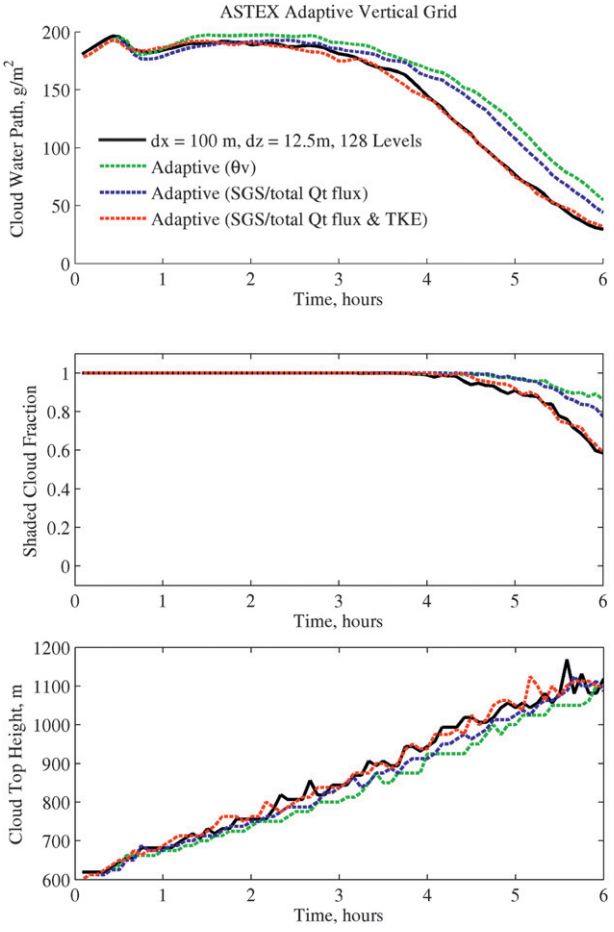

FIG. 7. Comparison of ASTEX (A209) simulations using a fixed vertical grid with a 12.5-m resolution with three adaptive vertical grid simulations. Panels are as in Fig. 1.

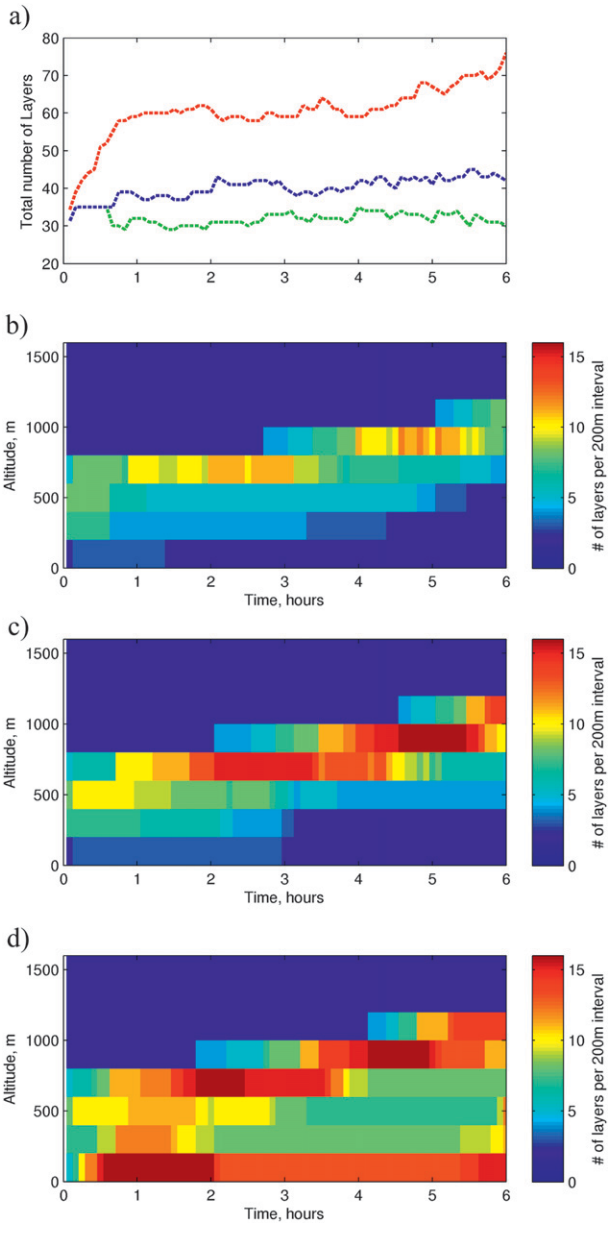

FIG. 8. As in Fig. 4, but for the ASTEX adaptive grid simulations.

These simulations (not shown) produced more cloud water and higher cloud fractions (than the 12.5-m simulations) but likewise showed somewhat less cloud water and lower cloud fractions than the fixed 6.25-m vertical grid simulation. It is unclear to what degree this is a result of the model spinup, and we suspect that this is at least partially a result of the fact that the temperature perturbations used in the model initializations have different scales due to the different starting grids (100 m × 100 m in the adaptive grid).

Figure 11 shows the vertical layer placement over time. The simulation with the potential temperature criterion (second panel) immediately adds vertical layers at the start of the simulation because the inversion exists from the outset. Clearly, a potential drawback of this criterion is that layers will be added near inversions whether or not they are needed to help simulate clouds. The simulation based on the SGS-to-total water flux criterion (third panel), on the other hand, adds layers between 600 and 800 m (near the cumulus cloud base) after the first hour and a short time later adds layers just above this level and then near the inversion (1400–1500 m). The reason for this delay is in part that (as described in section 2) we added a restriction to this criterion that requires that liquid water exists before a vertical layer can be added (to prevent spurious layers from being added where water content is low). If we remove this restriction (or change the restriction to a threshold based on total water rather than liquid water), layers are added to this simulations somewhat more rapidly. The simulation based on the SGS-to-total TKE and water flux criterion (bottom panel) immediately begins adding layers near the surface and within

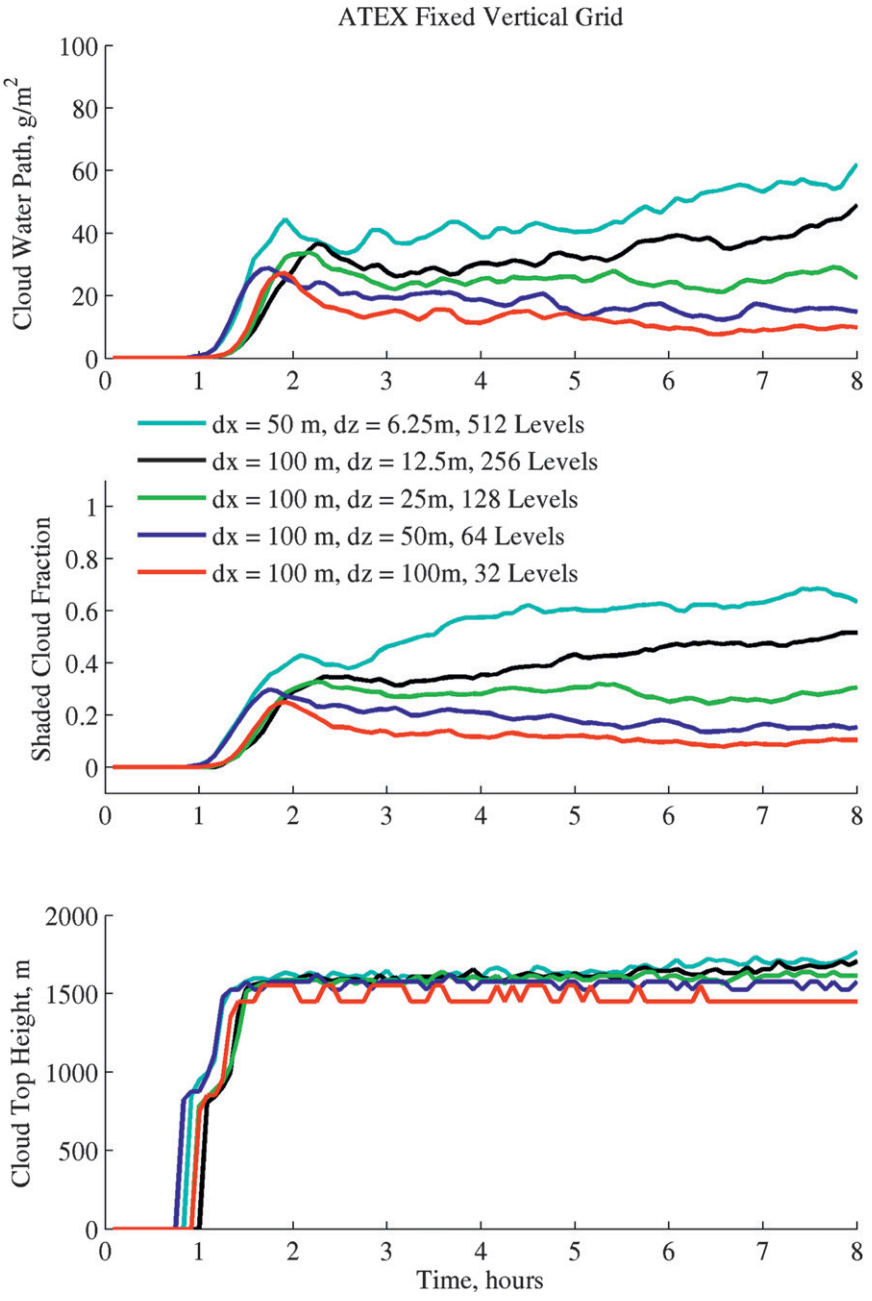

FIG. 9. As in Fig. 1, but for the ATEX simulations.

the first hour throughout (what will become) the subcloud layer, before cumulus clouds have developed.

6. Discussion

In this article we examined simulations using adaptive vertical grids for three well-studied stratocumulus cases based on three adaptive criteria: one criterion based on the change in potential temperature, one based on the ratio of subgrid-scale (SGS) to total water flux, and one based on SGS-to-total turbulent kinetic energy (TKE) and water flux. All three adaptive vertical grid simulations produced similar cloud water paths, cloud fractions, and cloud-top heights compared to simulations using a fixed vertical grid with fine grid spacing throughout the boundary layer. The cases examined cover a wide range of stratocumulus conditions including the transition from cumulus to patchy stratocumulus (ATEX), a physically thick stratocumulus under a strong inversion (ASTEX), and a thin stratocumulus deck transitioning into broken cumulus (DYCOMS-II).

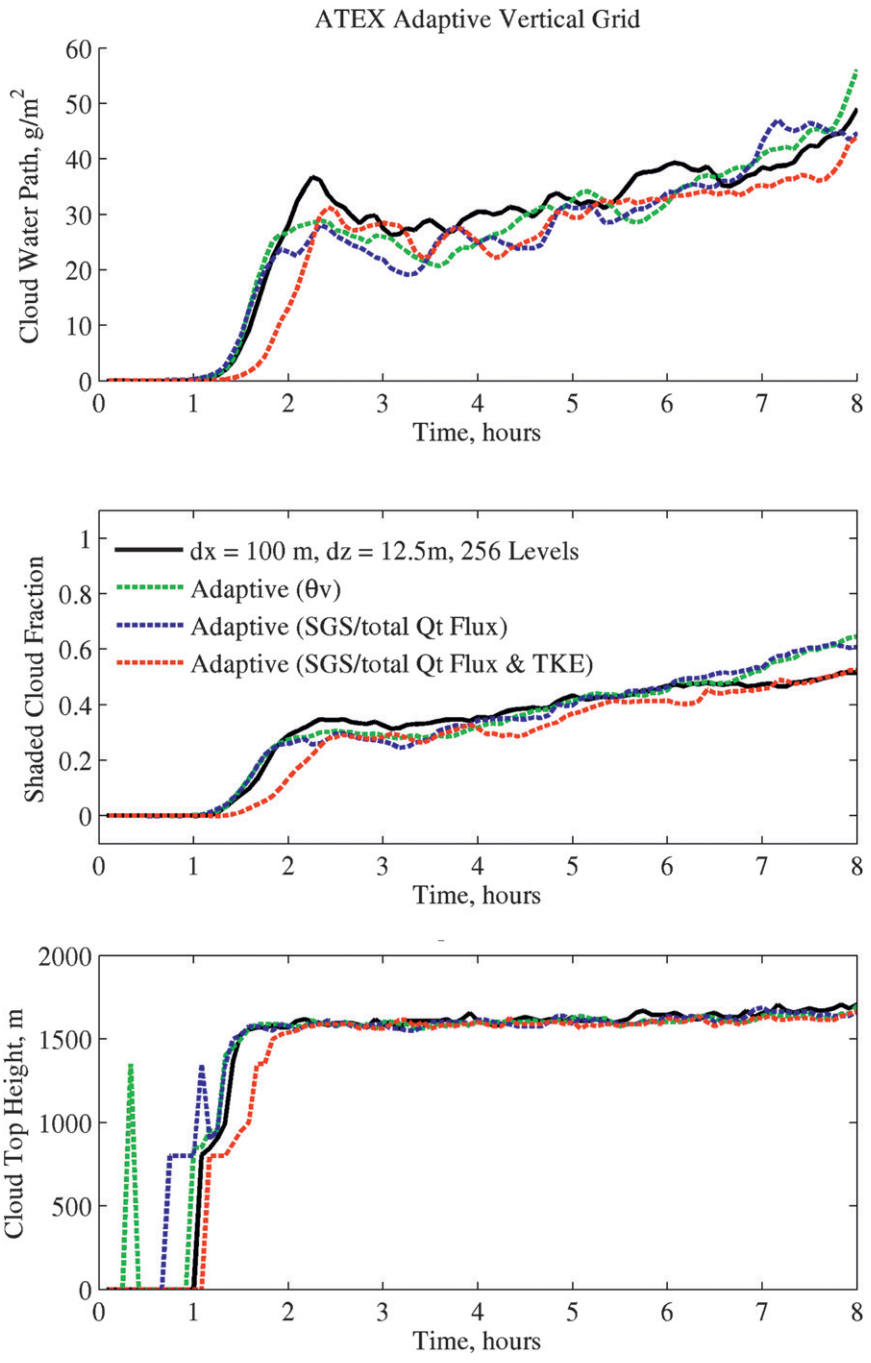

FIG. 10. As in Fig. 1, but for the ATEX simulations using a fixed vertical grid with a 12.5-m resolution with 3 adaptive vertical grid simulations.

It is encouraging that the adaptive vertical grid simulations performed well under this wide range of conditions. Nonetheless, more testing is needed. The simulations examined here are all two-dimensional (rather than three-dimensional), do not include shortwave radiation, and do not include drizzle. Our neglect of these factors is not because they are unimportant but rather because as a first step we sought to understand the behavior of the adaptive grid approach under relatively simple conditions and with sufficiently low computation burden that we could easily afford to undertake many simulations and test many potential adaptive criteria. The simulations are likewise short in duration and in some places it is difficult to determine if some observed differences are due to model

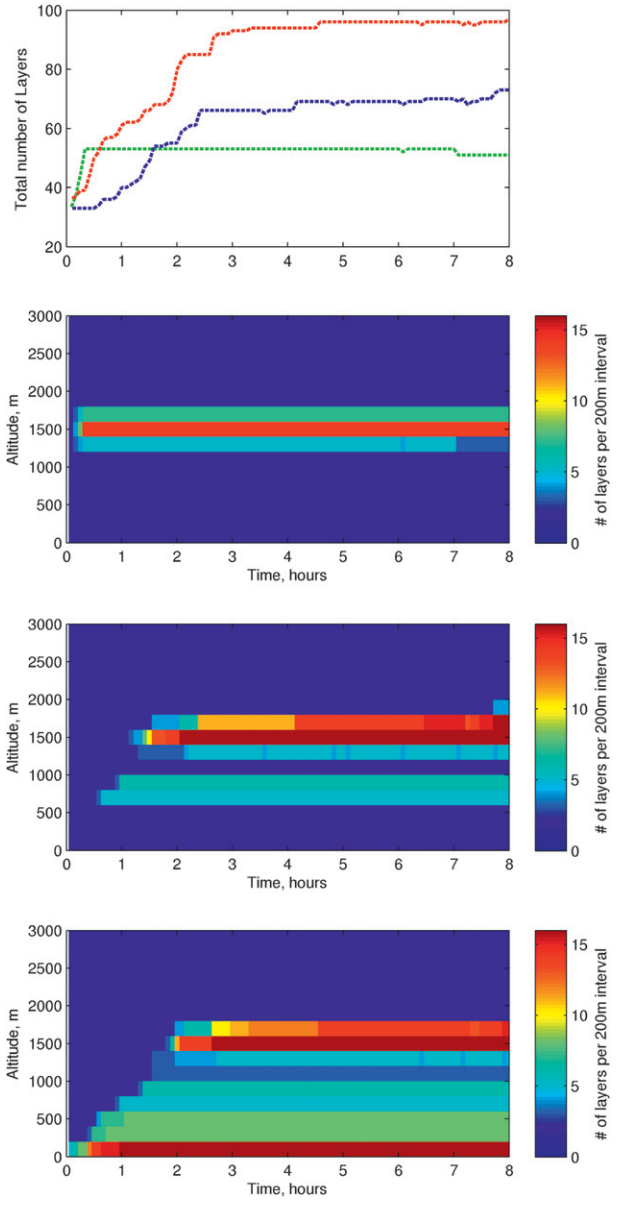

FIG. 11. As in Fig. 4, but for ATEX adaptive grid simulations.

initialization (or spinup) rather than reflecting limitations in the adaptive approach. In future research we plan to examine longer simulations that include multiple diurnal cycles.

While all of the adaptive grid simulations performed well, the simulations using the potential temperature and only the SGS-to-water flux criteria tended to maintain a more mixed (surface coupled) boundary layer and at times produced clouds with slightly higher cloud water paths and larger cloud fractions. The adaptive simulations using the SGS-to-total TKE and water flux criterion, on the other hand, were better able to reproduce the boundary layer structure, including decoupling in the subcloud layer. However, the improved representation comes at the cost of adding layers in the subcloud region. In the simulations presented here, the reduction in the total number of layers for the adaptive simulations using the SGS-to-total TKE and water flux criterion is only about a factor of 2. However, many of the layers added in the subcloud region are concentrated near the surface and we generally found that we could manually remove some of these near-surface layers and still model the subcloud layer well. Therefore, some refinement of this criterion that reduces the number of layers near the surface is likely possible. From the perspective of a climate model such as the Multiscale Modeling Framework (MMF), it is unclear how important it will be to represent the subcloud layer this well.

In the future we hope to add an adaptive grid capability to the MMF and test all three criteria. Most MMF simulations have been performed using a rather coarse 4-km horizontal grid. The adaptive criteria used here (at least the SGS-based criteria) are unlikely to work well with a horizontal grid spacing of 4 km. Even if the criteria do work, if we hold to an 8-to-1 length-to-width ratio limit, the gridcell vertical spacing would remain too large. However, we have run MMF simulations with horizontal grid spacings as fine as 250 m. These simulations were computationally expensive and limited to durations of a few months; nonetheless, we are confident that multiyear-long simulations with 250-m horizontal grid spacing and an adaptive grid will be possible in the very near future.

We stated earlier that the motivating idea behind all of the adaptive criteria (but especially the SGS-based criteria) is to minimize the dependence of the simulation on the subgrid-scale parameterization in favor of resolving turbulent motions. Cheng et al. (2010) found that the parameterized SGS total kinetic energy for coarse-resolution simulations is usually underestimated while the resolved total kinetic energy is unrealistically large, compared to benchmark (high resolution) simulations. These authors also found that they could artificially increase the eddy viscosity in the Smagorinsky–Lilly SGS parameterization to force this scheme to produce a similar level of SGS kinetic energy to the benchmark simulations, and that doing so resulting in a significant improvement in the simulation of the vertical transports of liquid water potential temperature and moisture when using a coarse-resolution grid. To a large degree, one can view the adaptive grid approach from this same perspective; the grid size becomes finer (where needed) in order to keep a reasonable SGS total kinetic energy (because the SGS scheme of SAM cannot predict realistic SGS total kinetic energy using a coarse grid) and thereby improves the simulation of vertical transports. With regard to the criterion that specifically

examines the SGS-to-total kinetic energy, this criterion results in layers being added in the subcloud region and improves vertical transports in this region, which is potentially important near the point where the cloud becomes decoupled from the surface layer.

In this study, our focus was on comparing the adaptive simulations to simulations with a fixed vertical grid rather than comparing to observations. This should in no sense be taken to suggest that because the SAM model cloud water path or cloud fractions converged (with decreases in the vertical grid spacing) this means the model has produced the correct answer. Stevens et al. (2001), for example, demonstrate that models with different numerics can converge to different answers. Rather, we would argue that one should not expect an adaptive grid version of any cloud-resolving model to produce better results than that model run with fine vertical grid spacing throughout the domain, and to the degree that such is observed it is a result of a cancellation of errors. The goal in developing an adaptive grid scheme should be to reproduce model simulations with fine vertical resolution everywhere while recognizing that this in no way reduces the importance of testing the model and ensuring that (when run with fine vertical resolution) it produces the right answers and for the right reasons. In particular, we note that in the DYCOMS-II case, the SAM model simulations (regardless of whether or not an adaptive grid is used) do not maintain a stratocumulus cloud as was observed during the field experiment, at least when run with vertical grid spacing as small as 5 m. Stevens et al. (2005) suggest that this occurred because of the particularly sensitive nature of this case and because SAM and other models they examined are numerically too diffusive. We anticipate that at some future point SAM may include less diffusive numerics. Cheng and Xu (2008), for example, are investigating the benefits of a higher-order turbulence scheme in SAM that could be coupled to an adaptive grid.

Acknowledgments. We thank Marat Khairoutdinov (Stony Brook University) for providing us with a copy of the System for Atmospheric Modeling (SAM). This research was supported by the U.S. Department of Energy (DOE) under Contract DE-AC06-76RL01830 and the National Science Foundation through the Center for Multiscale Modeling of Atmospheric Process (CMMAP) under Cooperative Agreement ATM-0425247.

APPENDIX

Formulation of Layer Insertion or Removal

The process of inserting or removing layer is depicted in Fig. A1. In this figure, the solid lines represent the interface between vertical grid cells. We start out with two neighboring grid cells of equal size labeled *a* and *b* (on the left side) and we add a layer labeled with an asterisk (on the right side) between these two layers. The superscript *a*, *b*, or * indicates the grid cell, while a subscript value of 1 indicates the initial two-layer state and a value of 2 the new three-layer state. In each grid cell the air density ρ; wind (momentum) components u, v, and w; absolute temperate T_{abs}; moist static energy t; total water mixing ratio q; total precipitating water mixing ratio q_p; and total kinetic energy (TKE) are assumed to be constant. The vertical location of each grid cell is defined by a variable z, which is located within the grid cell but is not necessarily located in the middle of the grid cell. Rather, we opt to define the location of the interface between grid cells as the midpoint between the neighboring grid cells' z values.

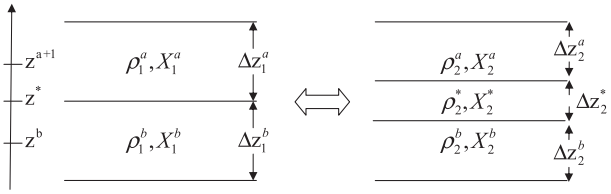

FIG. A1. Inserting or removing layers.

We add the new layer at the location of the interface between grid cells *a* and *b*, such that

$$z^* = 0.5(z^a + z^b). \tag{A1}$$

Consequently, the interface between grid cell *a* and the new layer is

$$\text{zi}^a_* = 0.5(z^a + z^*) = 0.75z^a + 0.25z^b,$$

the interface between grid cell *b* and the new layer is

$$\text{zi}^*_b = 0.5(z^b + z^*) = 0.25z^a + 0.25z^b,$$

and the width of the new layer is

$$\Delta z^*_2 = \text{zi}^a_* - \text{zi}^*_b = 0.5(z^a - z^b). \tag{A2}$$

The points z^a and z^b remain fixed as does the interface between grid cell *a* and the cell above it and likewise grid cell *b* and the cell below it. The size of grid cells *a* and *b* can likewise be calculated (from the distance between its interfaces as) on the left side of the figure (state 1 = only layers *a* and *b* exist) as

$$\Delta z^a_1 = 0.5(z^{a+1} - z^b) \quad \text{and} \tag{A3}$$

$$\Delta z_1^b = 0.5(z^a - z^{b-1}), \quad \text{respectively,} \tag{A4}$$

and on the right side of the figure (state 2 = three layers) as

$$\Delta z_2^a = 0.5(z^{a+1} - z^*) \quad \text{and} \tag{A5}$$

$$\Delta z_2^b = 0.5(z^* - z^{b-1}), \quad \text{respectively.} \tag{A6}$$

By conservation of mass, we expect

$$(\Delta z_1^a)\rho_1^a + (\Delta z_1^b)\rho_1^b = (\Delta z_2^a)\rho_2^a + (\Delta z_2^*)\rho_2^* + (\Delta z_2^b)\rho_2^b. \tag{A7}$$

where ρ is the air density. Choosing the density of grid cells a and b to be fixed (i.e., $\rho_1^a = \rho_2^a = \rho^a$) yields

$$(\Delta z_2^*)\rho^* = (\Delta z_1^a - \Delta z_2^a)\rho^a + (\Delta z_1^b - \Delta z_2^b)\rho^b.$$

Substituting (A1)–(A6) and simplifying, we find

$$\rho^* = 0.5(\rho^a + \rho^b). \tag{A8}$$

Similarly for the total water or precipitating water, conservation of mass gives

$$\begin{aligned}(X_1^a)(\Delta z_1^a)\rho_1^a + (X_1^b)(\Delta z_1)\rho_1^b = {} & (X_2^a)(\Delta z_2^a)\rho_2^a \\ & + (X_2^*)(\Delta z_2^*)\rho_2^* \\ & + (X_2^b)(\Delta z_2^b)\rho_2^b,\end{aligned}$$

where X is any gridcell mixing ratio. This in turn reduces to

$$X^*\rho^* = 0.5(X^a\rho^a + X^b\rho^b). \tag{A9}$$

Conservation of momentum and conservation of energy result in similar equations to (A8) and (A9) for other grid cell properties (e.g., the wind components, absolute temperature, moist static energy, water vapor mixing ratio, etc.).

Removing layers, we solve for variables on left side of figure given values on the right side. Equation (A7) still applies; however, in order to maintain conservation of mass and energy, we can no longer hold fixed air density in grid cells a and b. Substituting (A8) back into (A7) yields the following equations for the air densities in state 1:

$$(\Delta z_1^a)\rho_1^a = (\Delta z_2^a)\rho_2^a + (0.5\Delta z_2^*)\rho_2^*, \tag{A9}$$

$$(\Delta z_1^b)\rho_1^b = (\Delta z_2^b)\rho_2^b + (0.5\Delta z_2^*)\rho_2^*, \tag{A10}$$

and the water mixing ratios likewise become

$$(X_1^a)(\Delta z_1^a)\rho_1^a = (X_2^a)(\Delta z_2^a)\rho_2^a + (X_2^*)(0.5\Delta z_2^*)\rho_2^*, \tag{A11}$$

$$(X_1^b)(\Delta z_1^b)\rho_1^b = (X_2^b)(\Delta z_2^b)\rho_2^b + (X_2^*)(0.5\Delta z_2^*)\rho_2^*. \tag{A12}$$

It is interesting to note that in this formulation, if one adds a layer and then immediately removes the layer, one does not arrive back at the initial state. Rather, when we add a layer, we created region whose properties are weighted mixture of the properties from both initial grid cells a and b, and when we remove this layer we remix these properties back into a and b. Thus adding and then removing a layer effectively intermixes air from initial a and b grid cells.

Of course other formulations are possible. We have experimented with an alternative formulation where we add a new layer by simply dividing an initial grid cell into two equally sized halves (which start with identical gridcell properties) and likewise remove a layer by simply combining (and averaging properties) with a neighboring grid cell. In practice, this formulation performed worse than the one described above. The formulation given above also has the advantage that a given set of $(n + 1)$ z values completely specifies the vertical grid, while the alternative formulation is more difficult to implement because adding a layer requires shifting the position of already existing z grid points, as well as storing and tracking both the vertical gridpoint positions and the interface positions (since interface locations can no longer be defined simply as the midpoint between neighboring z values).

REFERENCES

Albrecht, B. A., C. S. Bretherton, D. W. Johnson, W. H. Schubert, and A. S. Frisch, 1995: The Atlantic Stratocumulus Transition Experiment—ASTEX. *Bull. Amer. Meteor. Soc.,* **76,** 889–904.

Bacon, D. P., N. Ahmad, T. J. Dunn, S. G. Gopalakrishnan, M. S. Hall, and A. Sarma, 2007: Hurricane track forecasting with OMEGA. *Nat. Hazards,* **41,** 457–470.

Barros, S. R. M., and C. I. Garcia, 2004: A global semi-implicit semi-Lagrangian shallow-water model on locally refined grids. *Mon. Wea. Rev.,* **132,** 53–65.

Bretherton, C. S., and Coauthors, 1999a: An intercomparison of radiatively driven entrainment and turbulence in a smoke cloud, as simulated by different numerical models. *Quart. J. Roy. Meteor. Soc.,* **125,** 391–423.

——, S. K. Krueger, M. C. Wyant, P. Bechtold, E. van Meijgaard, B. Stevens, and J. Teixeira, 1999b: A GCSS boundary layer model intercomparison study of the first ASTEX Lagrangian experiment. *Bound.-Layer Meteor.,* **93,** 341–380.

Cheng, A., and K.-M. Xu, 2008: Simulation of boundary-layer cumulus and stratocumulus clouds using a cloud-resolving model with low- and third-order turbulence closures. *J. Meteor. Soc. Japan,* **86A,** 67–86.

——, ——, and B. Stevens, 2010: Effects of resolution on the simulation of boundary-layer clouds and the partition of kinetic energy to subgrid scales. *J. Adv. Model. Earth Syst.,* **2** (3), doi:10.3894/JAMES.2010.2.3.

Deardorff, J. W., 1980: Stratocumulus-capped mixed layers derived from a three-dimensional model. *Bound.-Layer Meteor.,* **18,** 495–527.

de Roode, S. R., and P. G. Duynkerke, 1997: Observed Lagrangian transition of stratocumulus into cumulus during ASTEX: Mean state and turbulence structure. *J. Atmos. Sci.,* **54,** 2157–2173.

Dietachmayer, G. S., and K. K. Droegemeier, 1992: Application of continuous dynamic grid adaption techniques to meteorological modeling. Part I: Basic formulation and accuracy. *Mon. Wea. Rev.,* **120,** 1675–1706.

Duynkerke, P. G., H. Q. Zhang, and P. J. Jonker, 1995: Microphysical and turbulent structure of nocturnal stratocumulus as observed during ASTEX. *J. Atmos. Sci.,* **52,** 2763–2777.

——, and Coauthors, 1999: Intercomparison of three- and one-dimensional model simulations and aircraft observations of stratocumulus. *Bound.-Layer Meteor.,* **92,** 453–487, doi:10.1023/A:1002006919256.

Fiedler, B. H., and R. J. Trapp, 1993: A fast dynamic grid adaption scheme for meteorological flows. *Mon. Wea. Rev.,* **121,** 2879–2888.

Grabowski, W. W., 2001: Coupling cloud processes with the large-scale dynamics using the cloud-resolving convection parameterization (CRCP). *J. Atmos. Sci.,* **68,** 978–997.

Iselin, J. P., W. J. Gutowski, and J. M. Prusa, 2005: Tracer advection using dynamic grid adaptation and MM5. *Mon. Wea. Rev.,* **133,** 175–187.

Jablonowski, C., M. Herzog, J. E. Penner, R. C. Oehmke, Q. F. Stout, B. van Leer, and K. G. Powell, 2006: Block-structured adaptive grids on the sphere: Advection experiments. *Mon. Wea. Rev.,* **134,** 3691–3713.

Khairoutdinov, M. F., and Y. L. Kogan, 1999: A large-eddy simulation model with explicit microphysics: Validation against aircraft observations of a stratocumulus-topped boundary laye. *J. Atmos. Sci.,* **56,** 2115–2131.

——, and ——, 2000: A new cloud physics parameterization in a large-eddy simulation model of marine stratocumulus. *Mon. Wea. Rev.,* **128,** 229–243.

——, and D. A. Randall, 2003: Cloud resolving modeling of the ARM summer 1997 IOP: Model formulation, results, uncertainties, and sensitivities. *J. Atmos. Sci.,* **60,** 607–625.

Lauter, M., D. Handorf, N. Rakowsky, J. Behrens, S. Frickenhaus, M. Best, K. Dethloff, and W. Hiller, 2007: A parallel adaptive barotropic model of the atmosphere. *J. Comput. Phys.,* **223,** 609–628.

Marchand, R., and T. P. Ackerman, 2010: An analysis of cloud cover in multiscale modeling framework global climate model simulations using 4 and 1 km horizontal grids. *J. Geophys. Res.,* **115,** D16207, doi:10.1029/2009JD013423.

——, J. Haynes, G. G. Mace, T. Ackerman, and G. Stephens, 2009: A comparison of simulated cloud radar output from the multiscale modeling framework global climate model with CloudSat cloud radar observations. *J. Geophys. Res.,* **114,** D00A20, doi:10.1029/2008JD009790.

Randall, D., M. Khairoutdinov, A. Arakawa, and W. Grabowski, 2003: Breaking the cloud parameterizations deadlock. *Bull. Amer. Meteor. Soc.,* **84,** 1547–1564.

Skamarock, W. C., and J. B. Klemp, 1993: Adaptive grid refinement for two-dimensional and three-dimensional nonhydrostatic atmospheric flow. *Mon. Wea. Rev.,* **121,** 788–804.

Stevens, B., and Coauthors, 2001: Simulations of trade wind cumuli under a strong inversion. *J. Atmos. Sci.,* **58,** 1870–1891.

——, and Coauthors, 2003: On entrainment rates in nocturnal marine stratocumulus. *Quart. J. Roy. Meteor. Soc.,* **129,** 3469–3493.

——, and Coauthors, 2005: Evaluation of large-eddy simulations via observations of nocturnal marine stratocumulus. *Mon. Wea. Rev.,* **133,** 1443–1462.

Stevens, D. E., and C. S. Bretherton, 1999: Effects of resolution on the simulation of stratocumulus entrainment. *Quart. J. Roy. Meteor. Soc.,* **125,** 425–439.

——, A. S. Ackerman, and C. S. Bretherton, 2002: Effects of domain size and numerical resolution on the simulation of shallow cumulus convection. *J. Atmos. Sci.,* **59,** 3285–3301.

Zhang, Y., and Coauthors, 2008: On the diurnal cycle of deep convection, high-level cloud, and upper troposphere water vapor in the Multiscale Modeling Framework. *J. Geophys. Res.,* **113,** D16105, doi:10.1029/2008JD009905.